ACS OMEGA

http://pubs.acs.org/journal/acsodf
Article

Estrone-Based Derivatives Stabilize the *c-MYC* and *c-KIT* G-Quadruplex DNA Structures

Published as part of ACS Omega virtual special issue "Nucleic Acids: A 70th Anniversary Celebration of DNA".

Satendra Kumar, Annyesha Biswas, Sruthi Sudhakar, Divya Kumari, and Pushpangadan Indira Pradeepkumar*

Cite This: *ACS Omega* 2024, 9, 6616−6626
Read Online
ACCESS | Metrics & More | Article Recommendations | Supporting Information

ABSTRACT: G-rich sequences are present across the genome and can fold to form dynamic secondary structures, namely, G-quadruplexes (G4). These structures play a pivotal role in regulating numerous biological processes including replication, transcription, and translation. Therefore, targeting these structures using molecular scaffolds is an attractive approach to modulating their functions. Herein, we report the synthesis of three estrone-based derivatives (**Est-1**, **Est-2**, and **Est-3**) with a nonplanar core and a cationic alkyl side chain as G4 stabilizers. CD melting and polymerase stop assay results indicate that these ligands preferentially stabilize parallel *c-MYC* and *c-KIT1* G4s over the other G4s and duplex DNAs. The ligand **Est-3** shows cytotoxicity against cancer cell lines and effectively downregulates the *c-KIT* gene in HepG2 cell lines. Molecular modeling and dynamics studies showed that the ligand prefers stacking over the 5′-quartet of *c-MYC* G4 using the aromatic ring of the ligand. Overall, the findings of this study demonstrate that even G4 ligands can accommodate nonplanar scaffolds, which opens up new avenues for ligand design.

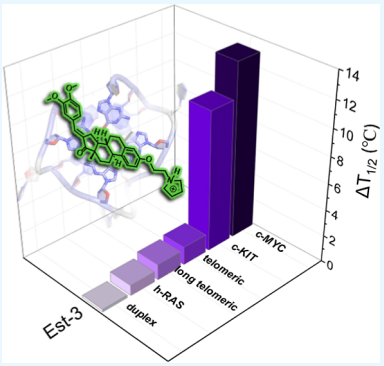

INTRODUCTION

In addition to double-stranded helical structure, DNA adopts numerous higher order structures, for instance, hairpin, triplex, G-quadruplex (G4), and i-Motif (iM).[1] Among these structures, G4 is the most extensively examined noncanonical structure of nucleic acids.[2,3] A G4 is formed by self-assembly of G-quartets which consist of four guanines arranged in a square-planar fashion held by Hoogsteen hydrogen bonding.[4−6] G4s are highly dynamic structures existing predominantly in three topologies: hybrid, parallel, and antiparallel (Figure 1).[4,5] The nature of DNA sequences, metal cations, types or length of loops, anti/syn sugar conformations, strand polarity, number of G-quartets, etc., are crucial factors in dictating a particular G4 topology.[4,7,8] G-rich sequences at the human telomeric regions principally form hybrid and antiparallel G4 structures in the K^+ and Na^+ ionic conditions, respectively.[9−11] The G-rich sequences of the oncogene promoter of *h-RAS* primarily form an antiparallel topology,[12] whereas the other promoters like *c-MYC*,[13] *c-KIT*,[14] *BCL-2*,[15] *PDGFR-β*,[16] *HIF-1α*,[17] *VEGF*,[18] etc., mostly form parallel G4 topologies. G4 formation at the telomeric end induces a series of DNA damage responses in cancerous cells leading to cell apoptosis.[19] The formation of stabilized G4 structure at the promoter region also attenuates the gene expression of oncogenes.[19] Since G4 structures are dynamic in nature, stabilizing them with small molecular scaffolds offers an avenue to develop anticancer drugs.

Many acridine, porphyrin, quinoline, phenanthroline, perylene diimide, polyheterocyclic macrocycles, naphthalene diimide, and fluoroquinolone-based scaffolds have been studied widely with various G4 DNA structures.[20−23] Most of these are conventional multimeric planar aromatic scaffolds; however, only limited nonplanar scaffolds utilizing steroid skeletons have been explored as G4 stabilizers.[22,24,25] This motivated us to design and synthesize estrone-based derivatives to study their interactions with G4 DNAs (Figure 2). The stabilization of G4 structures was evaluated using various biophysical, biochemical, and cellular studies. Moreover, molecular modeling and dynamic studies were employed to probe into the binding mode of the ligands with the G4 DNA.

RESULTS AND DISCUSSION

Ligand Design and Synthesis of Estrone-Based Derivatives. Estrone, which is an FDA-approved drug, is one of the estragons mainly used for the treatment of menopause, osteoporosis, and abnormalities associated with gonadotropin hormone dysfunction.[26,27] We designed estrone-based deriva-

Received: September 30, 2023
Revised: November 20, 2023
Accepted: November 28, 2023
Published: January 29, 2024

https://doi.org/10.1021/acsomega.3c07574
ACS Omega 2024, 9, 6616−6626

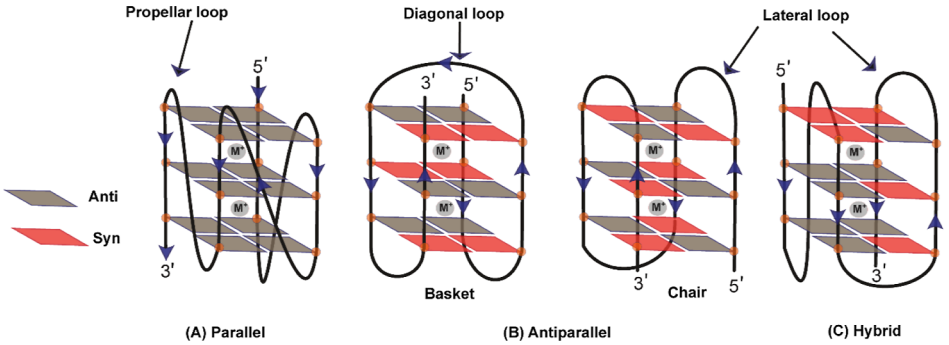

Figure 1. Various topologies and loops of the G4 DNA structures. The syn and anti orientation of nucleobases are shown in different colors.

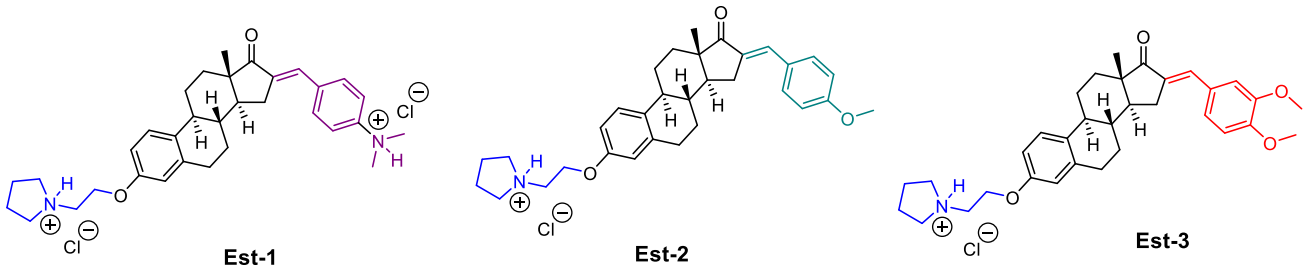

Figure 2. Structure of estrone-based derivatives used as G4 stabilizing ligands.

Scheme 1. Synthesis of Est-1, Est-2, and Est-3; Reagents and Conditions: (a) EtOH, 10% aq. NaOH, RT, 12 h; (b) 2-Chloro Ethyl Pyrrolidine Hydrochloride, Cs_2CO_3, ACN, Reflux, 24 h; and (c) HCl, DCM, 0 °C RT, 4 h

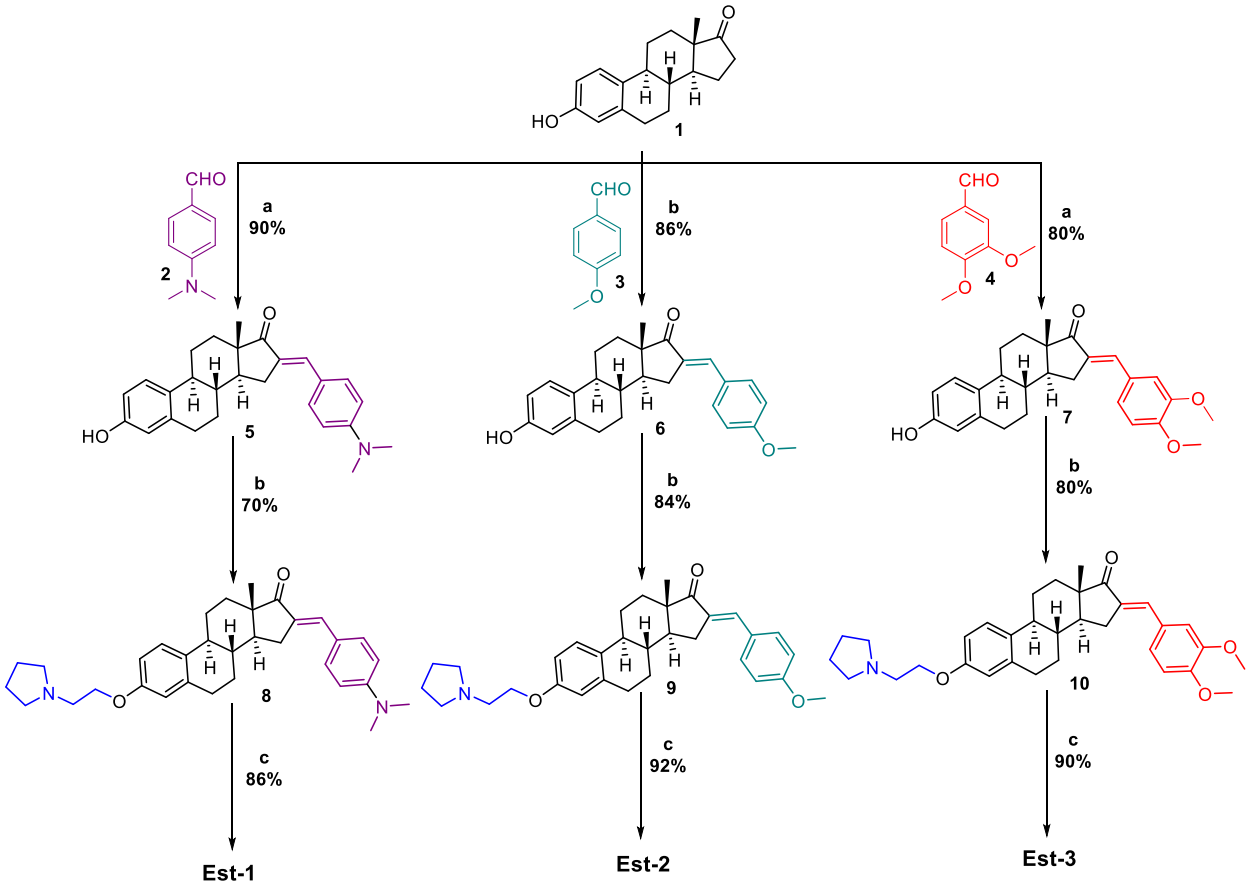

tives substituted with aromatic rings, which could enhance their interaction with the G-quartets (Figure 2). Moreover, the positive alkyl amine side chain was introduced to augment loop interactions and water solubility. Due to these unique structural features, we anticipated that these derivatives would show selectivity toward a particular G4 topology.[28]

https://doi.org/10.1021/acsomega.3c07574
ACS Omega 2024, 9, 6616−6626

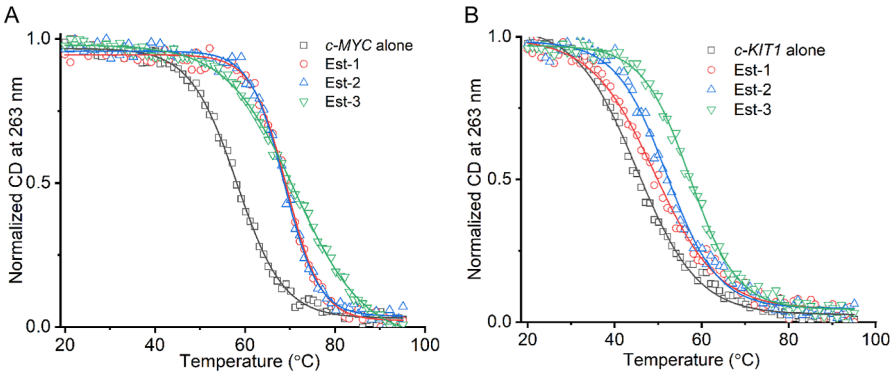

Figure 3. Normalized CD melting curves of *c-MYC* and *c-KIT1* G4 DNAs (10 μM G4 DNA in 10 mM lithium cacodylate buffer, pH 7.2) in the absence and presence of 5 mol equiv of ligands. (A) *c-MYC* (1 mM KCl and 99 mM LiCl) and (B) *c-KIT1* DNA (10 mM KCl and 90 mM LiCl).

Table 1. Thermal Stabilization of Various Quadruplex and Duplex DNAs Was Determined from CD Melting Experiments

ligands	[a]$\Delta T_{1/2}$					
	c-MYC	*c-KIT1*	telomeric	long telomeric	*h-RAS1*	duplex
Est-1	12.3 ± 0.8	7.0 ± 0.9	0.7 ± 0.3	0.9 ± 0.3	−2.0 ± 0.2	3.4 ± 0.8
Est-2	11.0 ± 0.6	7.9 ± 0.4	0.3 ± 0.4	1.6 ± 0.4	−1.2 ± 0.2	3.1 ± 1.1
Est-3	13.2 ± 0.4	10.6 ± 0.1	0.2 ± 0.4	1.4 ± 0.6	0.8 ± 0.3	1.2 ± 0.4

[a]$\Delta T_{1/2}$ represents the difference in the thermal melting temperature [$\Delta T_{1/2} = T_{1/2}$ (DNA + 5 mol equiv ligand) − $T_{1/2}$ (DNA)]. The reported values are the average of three independent experiments with estimated standard deviations. All the experiments were performed using 10 μM quadruplex DNA or 15 μM duplex DNA in 10 mM lithium cacodylate buffer, pH 7.2, in appropriate salt concentrations. The $T_{1/2}$ values in the absence of ligands are 57.2 ± 0.4 for *c-MYC* DNA, 44.7 ± 0.5 for *c-KIT1* DNA, 52.5 ± 0.2 for telomeric DNA in K^+ ion, 57.2 ± 0.2 for long telomeric DNA, 54.3 ± 0.2 for *h-RAS1* DNA, and 61.6 ± 0.5 for duplex DNA.

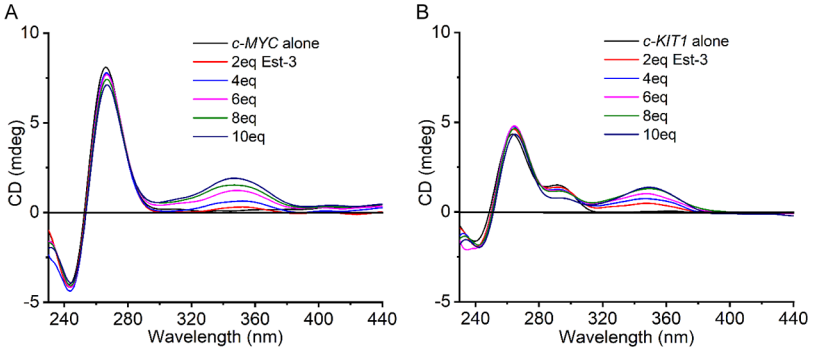

Figure 4. CD titration spectra of *c-MYC* and *c-KIT1* G4 DNAs (10 μM in 10 mM lithium cacodylate buffer, pH 7.2) with the **Est-3** ligand (0−100 μM). (A) *c-MYC* DNA (1 mM KCl and 99 mM LiCl) and (B) *c-KIT1* (10 mM KCl and 90 mM LiCl).

The synthetic strategy harnessed to obtain the estrone-based derivatives is shown in Scheme 1. Estrone derivatives **5**−**7** were synthesized by the base-mediated aldol condensation reaction of estrone (**1**) and different types of aldehydes (**2**−**4**) using a previously reported procedure with slight modifications.[29] In the presence of ethanolic NaOH, commercially available **1** was reacted with 4-dimethylamino benzaldehyde (**2**), 4-methoxy benzaldehyde (**3**), and 3,4-dimethoxy benzaldehyde (**4**) to yield compounds **5**, **6**, and **7** in 90, 86, and 80% yields, respectively. Compounds **5**−**7** were alkylated by 2-chloroethyl pyrrolidine hydrochloride using Cs_2CO_3 as a base to afford compounds **8**, **9**, and **10** in 70, 84, and 80% yield, respectively. Finally, compounds **8**−**10** were protonated with HCl to enhance the solubility to afford **Est-1**, **Est-2**, and **Est-3** in 86, 92, and 90% yields, respectively.

Circular Dichroism Melting Studies. Circular dichroism (CD) melting experiment was employed to investigate the effect of the ligands on the thermal stability of G4s and duplex DNA.[30] The melting studies were performed using 10 μM G4 and 15 μM duplex DNAs in the absence and presence of estrone ligands by monitoring the CD intensity at the appropriate wavelengths using suitable salt and buffer concentrations. The addition of up to 5 mol equiv of the estrone ligands (**Est-1**−**3**) to *c-MYC* G4 DNA (Figure 3A and Table 1) exhibited a substantial increment in melting temperature ($\Delta T_{1/2}$ = 11−13 °C). Likewise, these ligands significantly increased the melting temperature of the *c-KIT* G4 DNA in the presence of **Est-3** ($\Delta T_{1/2}$ = 10.6 °C), followed by **Est-2** ($\Delta T_{1/2}$ = 7.9 °C) and **Est-1** ($\Delta T_{1/2}$ = 7.0 °C) (Figure 3B and Table 1). Further, to deduce the extent of thermal stabilization imparted by these ligands toward various DNAs, thermal melting studies were also performed using telomeric, long telomeric, *h-RAS1*, and duplex DNAs (Figure S1A−D, Supporting Information and Table 1). The thermal denaturation profile of hybrid telomeric, long telomeric, *h-RAS1* G4, and duplex DNAs displayed negligible changes in the

https://doi.org/10.1021/acsomega.3c07574
ACS Omega 2024, 9, 6616−6626

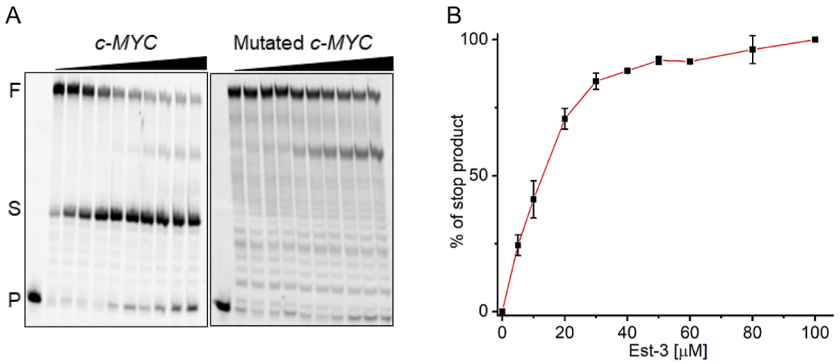

Figure 5. 15% denaturing PAGE (7 M urea) of *Taq* DNA polymerase stop assay of the *c-MYC* and mutated *c-MYC* DNAs with an increasing concentration of **Est-3** (0−100 μM). (A) *c-MYC* and mutated *c-MYC* template DNAs and (B) plot of the percentage of the stop product against the increasing concentration of **Est-3** ligand. F, S, and P denote the full length, stop product, and primer, respectively.

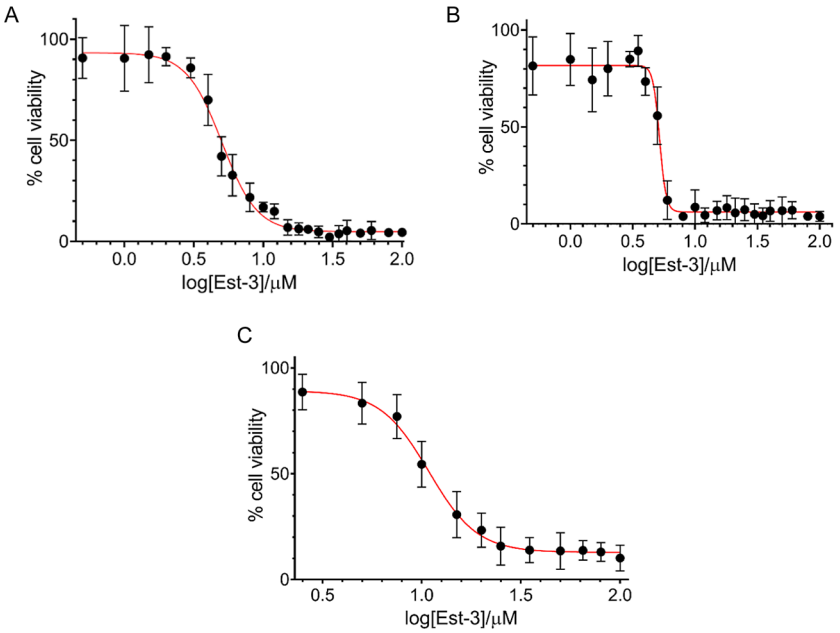

Figure 6. Plot for the % cell viability by the MTT assay. (A) HeLa, (B) HepG2, and (C) Lenti-X cell lines with increasing concentration of **Est-3** (0−100 μM). The curve was fitted by using the dose−response equation; error bars represent the standard deviations derived from three independent experiments.

melting temperature in the presence of all the three ligands (Table 1 and Figure S1A−D, Supporting Information).

Therefore, comprehensive CD melting studies indicated that **Est-1−3** ligands preferentially stabilized the parallel topologies of *c-MYC* and *c-KIT1* G4s over other topologies of G4 DNAs as well as duplex DNA. Since **Est-3** showed maximum thermal stabilization with G4 DNAs, it was selected for further biophysical, biochemical, molecular modeling, and cellular studies.

CD Titration Studies. The addition of **Est-3** to the *c-MYC* and *c-KIT1* G4 DNAs did not induce any change in the position of the positive peak at 260 nm and the negative peak at 240 nm in the CD spectra, suggesting retention of parallel topology (Figure 4A,B).[30] The addition of increasing concentration of **Est-3** to the *h-RAS1* G4 DNA displayed retention of the positive peak at 290 nm and the negative peak at 260 nm in K^+ ions, consistent with the antiparallel G4 topology (Figure S2A, Supporting Information). The hybrid topology of telomeric G4 DNA in K^+ ions showing a negative peak at 295 nm and a positive peak at 240 nm along with a shoulder peak at 260 nm was also preserved while titrating with **Est-3** (Figure S2B, Supporting Information).

Notably, a weak positive ICD signal was observed in the CD spectra of all G4-forming DNA at around 400−320 nm upon the addition of increasing concentration of ligand (Figures 4A,B and S2A,B, Supporting Information). The absorption peak of the **Est-3** ligand is at 380 nm, found in the same region as the ICD signal in the CD spectra. The ICD peak in the CD spectra of all G4s can be observed due to the interaction of the chiral ligand with circularly polarized light (Figure S3A,B, Supporting Information).[31] Therefore, overall CD titration results showed that **Est-3** neither destroys nor alters any of the fundamental topologies of G4 DNA structures.

***Taq* DNA Polymerase Stop Assay.** In the absence of added **Est-3**, stop products were not observed in any reaction mixture containing telomeric, *c-MYC*, and mutated *c-MYC* DNAs as the G4 structures formed were unfolded by the *Taq* polymerase enzyme (Figures 5A and S4, Supporting Information). The findings of the CD melting experiment suggested the preferential stabilization of parallel G4 DNAs in the presence

https://doi.org/10.1021/acsomega.3c07574
ACS Omega 2024, 9, 6616−6626

of the **Est-3** ligand; likewise, in the presence of this ligand, stop product formation was also observed with *c-MYC* DNA (Figure 5A). When the **Est-3** concentration was plotted against % stop product formation, an IC_{50} value of ∼10 μM was obtained (Figure 5B). The stop product formation was not clearly evident in the case of telomeric or mutated *c-MYC* DNAs even after subsequent addition of up to 100 μM ligand concentration (Figures 5A and S4, Supporting Information). Thus, the *Taq* DNA polymerase stop assay further corroborated the results obtained from the CD melting studies.

Cell Viability and Gene Downregulation Studies. The cell viability assay was carried out using the MTT assay to evaluate the cytotoxic effect of **Est-3** on cancerous human cervical (HeLa) cells, liver hepatocellular (HepG2) cells, and noncancerous (Lenti-X) cell line.[32] *c-MYC* and *c-KIT* genes are overexpressed in HeLa and HepG2 cancer cells, respectively. Since ligand **Est-3** showed the highest stabilization with *c-MYC* and *c-KIT* G4 DNAs, cellular studies have been performed with these cancer cell lines.[33,34] After 24 h, **Est-3** exhibited a low IC_{50} value against HeLa and HepG2 cell lines ∼5.0 ± 0.1 and ∼5.2 ± 0.1 μM, respectively (Figure 6A,B), as compared to Lenti-X (∼10.9 ± 0.6 μM) (Figure 6C) cells. Thus, ligand **Est-3** demonstrated almost 2-fold higher toxicity toward cancerous cell lines compared to the noncancerous cells.

Further, the qRT-PCR experiment was employed to examine the effect of **Est-3** on gene expression of the *c-KIT* gene in HepG2 cell lines at the transcriptional level.[35] These cells were treated with the IC_{50} value (5 μM) of **Est-3** and incubated over a period of 48 h. β-Actin, a housekeeping gene, was used as a control, and the expression of HepG2 mRNA was normalized against this gene. The findings of the qRT-PCR assay indicated 2.5-fold repression of the mRNA level of the *c-KIT* gene by the **Est-3** ligand (Figure 7). In summary, **Est-3** showed cytotoxicity toward cancerous cells and downregulated *c-KIT* gene expression.

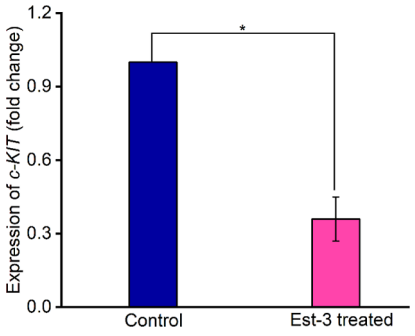

Figure 7. Effects of the **Est-3** ligand (5 μM) on the expression of the *c-KIT* gene in HepG2 cell lines from qRT-PCR after 48 h of treatment. The fold change is calculated using the $2^{(-\Delta\Delta Ct)}$ method. Error bars represent the standard deviations derived from three independent experiments. The *p*-value was evaluated by Student's *t*-test. * $p < 0.05$, which was considered a significant difference compared to untreated cells (control).

Molecular Modeling and Dynamics Studies. To study the binding modes and noncovalent interactions between the ligand **Est-3** and *c-MYC* G4 DNA, molecular modeling and dynamics studies were conducted. The energy-optimized structure (Figure S5) was docked with the *c-MYC* G4 DNA. The most populated clusters displayed the groove binding mode and stacking at the 5′-end of G4. Representative low-energy conformers from these clusters were chosen as starting structures for 500 ns molecular dynamics (MD) simulations (Figure S6).

MD simulation of the groove-bound structure showed that **Est-3** falls off from the DNA after 100 ns and then shows a weak interaction at the 3′-end (Figure S7). Due to this inefficient binding of the groove-bound conformer, only the complex with the ligand stacking at the 5′-end was utilized for further analysis. The root-mean-square deviation (RMSD) of the ligand, the backbone of the DNA, and G-quartets were initially calculated with respect to the first frame of the simulation (Figure 8A). The

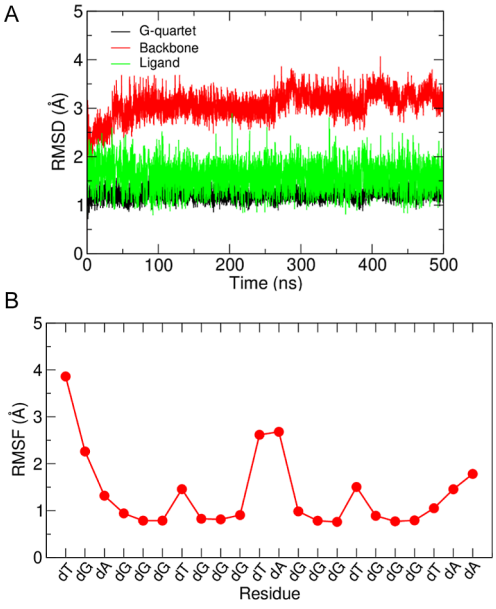

Figure 8. (A) Time-dependent RMSD values of the G-quartet, DNA backbone atoms, and the ligand. The RMSD of the G-quartet is represented in black, backbone atoms in red, and the ligand in green; (B) RMSF plot of the ligand-bound *c-MYC* G4 DNA. The graphs plotted are fluctuations of the nucleotides numbered from 5′ to 3′. The calculations are performed using all the frames of the 500 ns trajectory.

ligand and G-quartets showed stable and low RMSD values, indicating minimal changes from their initial orientation. The average value of backbone RMSD is higher than that of the G-quartet alone (Figure S8), suggesting that the flanking and loop nucleotides undergo large fluctuations during the simulation. The root-mean-square fluctuations (RMSF) of all the nucleotides were calculated to explore this further. The RMSF values of the quartet forming dG residues are <1 Å, while the 5′-end flanking nucleotides, loop nucleotides, and 3′-end flanking nucleotides showed values up to 4, 3, and 2 Å, respectively (Figure 8B). This suggests that the maximum reorientation happens at the 5′-end, where the flanking nucleotides rearrange to accommodate the ligand.

The simulation trajectory was clustered to understand the population distribution of the G4-**Est-3** conformations. Out of the five clusters generated, cluster 1 occurred for ∼90% of the simulation time. The visual inspection of the representative structure revealed that the ligand was stacked over the top quartet at the 5′-end (Figure 9A). The two aromatic moieties in **Est-3** participate in the stacking interaction with the G-quartet. While the aromatic part of the estrone core is stacked over dG8 of the top quartet (Figure 9B), the dimethoxybenzyl group is stacked over dG17 of the top quartet (Figure 9C). The

https://doi.org/10.1021/acsomega.3c07574
ACS Omega 2024, 9, 6616−6626

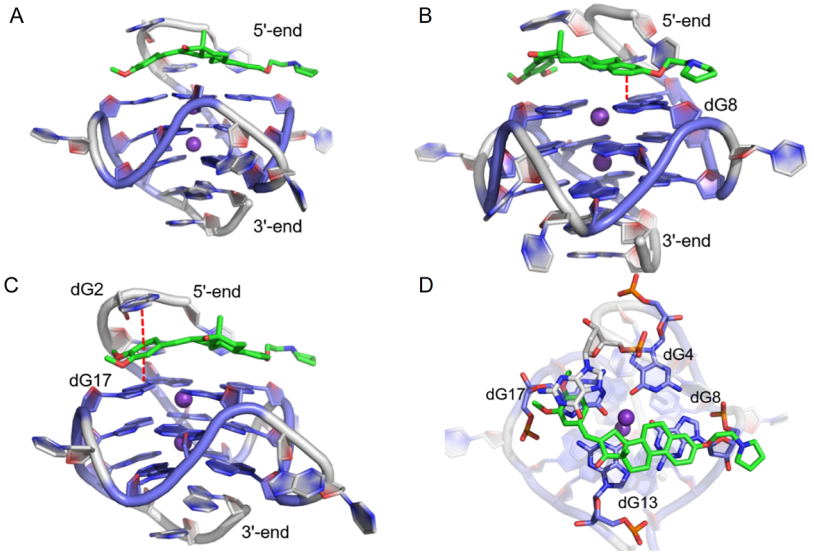

Figure 9. Representative structure of the major cluster of the **Est-3**-*c-MYC* G4 DNA complex. (A) Side view of the major cluster showing the stacking at 5′-end of G4 DNA; (B) image showing the stacking interaction of the estrone aromatic moiety with G4 DNA; (C) image showing the stacking interaction of the dimethoxybenzyl moiety with the G4 DNA; and (D) axial view of the representative structure of the major cluster of the complex. The carbon atoms of the ligand are represented in green, G-quartet in purple, flanking and loop nucleotides in white, phosphorus in orange, oxygen in red, and nitrogen in blue. The K^+ ions in the G4 core are represented as violet spheres.

dimethoxybenzyl group also engages in a stacking interaction with the flanking nucleotide, dG2 (Figure 9C). The alicyclic part of the estrone core partially covered the dG8 and dG13 nucleotides of the top quartet (Figure 9D).

To gain a better understanding of the noncovalent interactions present in the **Est-3**-G4 complex, the stacking, van der Waals (vdW), and electrostatic interactions were explored. Due to the minimal reorientation of the ligand, there is no prominent electrostatic interaction with the DNA. However, as evident from the cluster analysis, there are multiple stacking interactions of the different aromatic moieties of the ligand with various nucleotides as discussed above. Stacking distances and vdW energy contributions of the ring moieties were calculated separately (Table S4).

All of the stacking distances remained below 5 Å, and the energy contributions were equal. This indicates that both the dimethoxybenzyl and estrone core aromatic moieties equally contribute to the stacking interactions. The radial distribution function was estimated to understand the propensity of the interaction of the dimethoxybenzyl moiety with the flanking and quartet dG residues (Figure S9). The radial distribution functions are almost identical, indicating that the dimethoxybenzyl ring equally engages in π-stacking with both the dG2 and dG17 nucleotides. The vdW interaction energy of the ligand and the top quartet was found to be -34.5 ± 2.3 kcal/mol. The linear interaction energy of the alicyclic part of the estrone core with the top quartet was also calculated separately. The alicyclic part exhibited a vdW energy of -13.2 ± 1.2 kcal/mol, showing the involvement of this moiety in stabilizing the G-quartet at the 5′-end.

The binding energy of the ligand with *c-MYC* G4 was estimated by using the MM/PBSA calculation (Table S5). The total binding energy is -23.8 ± 7.2 kcal/mol, with the total enthalpic contribution being -43.6 ± 3.5 kcal/mol and the entropic contribution being -19.8 ± 7 kcal/mol. This indicates that the binding of **Est-3** on *c-MYC* G4 is an enthalpy-driven process. From MD simulations, it is clear that the preferred binding mode of the ligand is stacking at the 5′-end of G4 DNA involving the aromatic moieties along with stabilizing vdW interactions from the alicyclic part of the estrone core. The stacking interactions of the aromatic residues with the flanking nucleotides further stabilize the binding to the G4 structure.

Summary and Conclusions. In summary, a series of estrone-based ligands compromising the nonplanar core were synthesized. These ligands preferentially stabilized the *c-MYC* and *c-KIT1* promoter G4 DNAs over other G4 and duplex DNAs, as confirmed by biophysical and biochemical studies. MD studies revealed that the aromatic cores of **Est-3** stabilize the stacking interactions, while the alicyclic part engages in stabilizing vdW interactions with G4 DNA. **Est-3** exhibited cytotoxicity against cancer cells and downregulated *c-KIT* gene expression in HepG2 cells at the transcriptional level. In summary, the overall findings of our studies showed that the estrone-based ligands can be utilized as G4 stabilizers, which offers new opportunities to design G4 ligands for therapeutic applications.

EXPERIMENTAL SECTION

General Experimental Details. The solvents and chemicals employed in the synthesis were purchased from Sigma-Aldrich, TCI-Japan, Alfa Aesar-UK, Merck-India, Spectrochem-India, and Finar-India. All chemicals and ethanol were used without further purification, whereas acetonitrile was dried by CaH_2 and stored at 4 Å molecular sieves for 24 h before using in the reaction. The progress of reactions was monitored with the help of thin layer chromatography (TLC) under UV light (260 nm) using silica gel plates precoated with fluorescent indicators. Silica gel (100−200 mesh) or neutral alumina (60−325 mesh) was used as the stationary phase to perform column chromatography. The ^1H and ^{13}C spectra of all purified compounds were recorded on 400 or 500 MHz Bruker (Germany) AVANCE III NMR instruments. Chemical shift values in parts per million (ppm) were reported downfield to the TMS signal (0 ppm) and referenced from the TMS signal or deuterated residual solvents: $CDCl_3$ (7.26 ppm), CD_3OD (3.31 ppm), DMSO-d_6 (2.5 ppm), and D_2O (4.79 ppm) for ^1H NMR

https://doi.org/10.1021/acsomega.3c07574
ACS Omega 2024, 9, 6616−6626

spectra and $CDCl_3$ (77.2 ppm), CD_3OD (49.1 ppm), and DMSO-d_6 (39.5 ppm) for ^{13}C NMR spectra. ^1H NMR spin coupling multiplicities are stated as s (singlet), d (doublet), t (triplet), dd (doublet of doublets), and (q) quintet or m (multiplet and overlapping spin systems). The apparent coupling constant (J) values are given in hertz (Hz). A Q-TOF analyzer was utilized to record high-resolution mass spectra (HRMS) (Maxis Impact Bruker) in positive-ion electrospray ionization (ESI) mode. The oligonucleotides used in biophysical and biochemical studies were synthesized in-house using a H6 DNA/RNA Synthesizer (K & A lab GMBH). The synthesized oligonucleotides were purified with 15 or 20% desaturating polyacrylamide gel (PAGE). Human cervical cancer cell lines (HeLa), liver hepatocellular cancer cell lines (HepG2), and human kidney cell lines (Lenti-X) were acquired from NCCS, Pune. All dNTPs, *Taq* polymerase, verso cDNA synthesis kit, and Gene JET RNA purification kit were procured from Thermo Scientific, whereas ExcelTaqTM 2X Q-PCR Master Mix (SYBR, ROX) was obtained from SMOBiO Technology. The media, serum, antibiotics, trypsin, PBS, and other reagents utilized in the cell-based experiments were acquired from HiMedia, MP Biomedicals, and Gibco.

Synthetic Procedures. *General Procedure for the Preparation of Aldol Products (**5**, **6**, and **7**). Method **A**.* An appropriate amount of estrone **1** (1 equiv) and aldehyde **2**−**4** (1.2 equiv) was dissolved in ethanol. To this solution was added 10% aqueous KOH, allowing the reaction mixture to stir at room temperature for over 12 h. The reaction mixture was then poured into cold water and neutralized with a few drops of acetic acid to obtain a precipitate. The obtained residue was further washed with cold water to furnish a pure solid compound.

*General Procedure for the Preparation of Alkylated Products (**8**, **9**, and **10**). Method **B**.* 1 equivalent of aldol product (**5**−**7**) was dissolved in dry ACN with 4 equiv of Cs_2CO_3 and stirred at room temperature under nitrogen conditions. To this solution, 2-chloroethyl pyrrolidine hydrochloride (2 equiv) was added and refluxed at 80 °C for 24 h to get alkylated products. After completion of the reaction, the reaction mixture was allowed to stand at room temperature and extracted with EtOAc (2 × 100 mL). The obtained crude products were then purified using column chromatography in a silica gel stationary phase to afford the pure product.

*General Procedure for the Preparation of Protonated Compounds (**Est-1, Est-2, and Est-3**). Method **C**.* 1 equivalent of the alkylated product (**1**−**10**) was dissolved in DCM and stirred at 0 °C. To this solution, 10 equiv of concentrated HCl was added and stirred for 4 h to get a protonated solid residue. The residue was washed thrice with DCM and diethyl ether to obtain pure protonated products.

(8*R*,9*S*,13*S*,14*S*)-16-((*E*)-4-(Dimethylamino)-benzylidene)-3-hydroxy-13-methyl-6,7,8,9,11,12,13,14,15,16-decahydro-17*H*-cyclopenta[*a*]phenanthren-17-one (5). Compound **5** was prepared as an orange solid by employing method **A** by the reaction of estrone **1** (100 mg, 0.37 mmol) and 4-dimethylaminobenzaldehyde **2** (66.2 mg, 0.44 mmol); mp 295 to 300 °C; yield 90% (134 mg); R_f = 0.5 (30% ethyl acetate in pet ether). ^1H NMR (400 MHz, DMSO-d_6): δ 9.22 (s, 1H), 7.45 (d, J = 8.8 Hz, 2H), 7.18 (s, 1H), 7.03 (d, J = 8.4 Hz, 1H), 6.73 (d, J = 8.8 Hz, 2H), 6.51 (dd, J = 8.3, 2.5 Hz, 1H), 6.45 (d, J = 2.5 Hz, 1H), 2.95 (s, 6H), 2.83−2.73 (m, 2H), 2.44−2.13 (m, 3H) 1.95−1.81 (m, 2H), 1.56−1.32 (m, 5H), 1.04 (t, J = 7.0 Hz, 1H), 0.83 (s, 3H). ^{13}C NMR (100 MHz, DMSO-d_6): δ 209.6, 155.2, 151.3, 137.7, 133.6, 132.6, 130.9, 130.7, 126.5, 122.7, 115.4, 113.2, 112.3, 56.6, 48.6, 47.4, 43.8, 37.9, 31.8, 29.4, 29.1, 26.7, 26.0, 18.8, 14.9, HRMS (ESI): calcd for $C_{27}H_{32}NO_2$: $[M + H]^+$, 402.2428; found: $[M + H]^+$, 402.2423 (Δm = +0.0005 and error = +1.2 ppm).

(8*R*,9*S*,13*S*,14*S*)-3-Hydroxy-16-((*E*)-4-methoxybenzylidene)-13-methyl-6,7,8,9,11,12,13,14,15,16-decahydro-17*H*-cyclopenta[*a*]phenanthren-17-one (6). Compound **6** was prepared as a yellow solid employing method **A** by the reaction of estrone **1** (100 mg, 0.37 mmol) and 4-methoxybenzaldehyde **3** (66.0 mg, 0.44 mmol); mp 260 to 266 °C; yield 86% (123 mg); R_f = 0.62 (30% ethyl acetate in pet ether). ^1H NMR (400 MHz, $CDCl_3$): δ 7.52 (d, J = 8.7 Hz, 2H), 7.44 (s, 1H), 7.16 (d, J = 8.4 Hz, 1H), 6.95 (d, J = 8.7 Hz, 2H), 6.66 (dd, J = 8.4, 2.6 Hz, 1H), 6.61 (d, J = 2.5 Hz, 1H), 5.31 (s, 1H), 3.85 (s, 3H), 2.99−2.88 (m, 3H), 2.54−2.46 (m, 1H), 2.43−2.37 (m, 1H), 2.32−2.26 (m, 1H), 2.10−2.05 (m, 2H), 1.75−1.43 (m, 6H), 1.0 (s, 3H). ^{13}C NMR (100 MHz, $CDCl_3$): δ 210.2, 160.5, 153.7, 137.9, 133.5, 133.3, 132.1, 132.0, 128.3, 126.4, 115.3, 114.2, 112.9, 55.4, 48.7, 47.8, 44.0, 37.9, 31.7, 29.5, 29.1, 26.8, 26.0, 14.6, HRMS (ESI): calcd for $C_{26}H_{29}NO_3$: $[M + H]^+$, 389.2111; found: $[M + H]^+$, 389.2112 (Δm = −0.0001 and error = −0.1 ppm).

(8*R*,9*S*,13*S*,14*S*)-16-((*E*)-3,4-Dimethoxybenzylidene)-3-hydroxy-13-methyl-6,7,8,9,11,12,13,14,15,16-decahydro-17*H*-cyclopenta[*a*]phenanthren-17-one (7). Compound **7** was prepared as a yellow solid by employing method **A** by the reaction of estrone **1** (100 mg, 0.37 mmol) and 3,4-dimethoxybenzaldehyde **4** (73.0 mg, 0.44 mmol); mp 220 to 230 °C; yield 80% (124 mg); R_f = 0.68 (30% ethyl acetate in pet ether). ^1H NMR (500 MHz, $CDCl_3$): δ 7.45 (s, 1H), 7.23−7.18 (m, 2H), 7.11 (s, 1H), 6.95 (d, J = 8.3 Hz, 1H), 6.69 (dd, J = 8.3, 2.5 Hz, 1H), 6.64 (s, 1H), 5.32 (s, 1H), 3.95 (s, 6H), 3.03−2.90 (m, 3H), 2.57−2.30 (m, 3H), 2.12−2.07 (m, 2H), 1.77−1.58 (m, 5H), 1.54−1.48 (m, 1H), 1.02 (s, 3H). ^{13}C NMR (125 MHz, $CDCl_3$): δ 210.0, 153.7, 150.2, 148.9, 137.9, 133.8, 133.5, 131.9, 128.6, 126.5, 124.0, 115.3, 113.3, 112.9, 111.1, 55.9, 48.7, 47.8, 44.1, 37.9, 31.7, 29.5, 29.0, 26.8, 26.0, 14.6, HRMS (ESI): calcd for $C_{26}H_{29}NO_3$: $[M + H]^+$, 419.2217; found: $[M + H]^+$, 419.2203 (Δm = +0.0014 and error = +3.3 ppm).

(8*R*,9*S*,13*S*,14*S*)-16-((*E*)-4-(Dimethylamino)-benzylidene)-13-methyl-3-(2-(pyrrolidin-1-yl)ethoxy)-6,7,8,9,11,12,13,14,15,16-decahydro-17*H*-cyclopenta-[*a*]phenanthren-17-one (8). Compound **8** was prepared by employing method **B** by the reaction of compound **5** (50 mg, 0.12 mmol) and 2-chloroethyl pyrrolidine hydrochloride using a Cs_2CO_3 (162 mg, 0.5 mmol) base. The crude product was purified with the aid of column chromatography (10% MeOH in DCM) using silica gel to afford pure compound **8** as a yellow solid; mp 270 to 274 °C; yield 70% (48 mg); R_f = 0.26 (80% ethyl acetate in pet ether). ^1H NMR (400 MHz, $CDCl_3$): δ 7.48 (d, J = 8.7 Hz, 2H), 7.41 (s, 1H), 7.20 (d, J = 8.5 Hz, 1H), 6.74−6.68 (m, 4H), 4.10 (t, J = 6 Hz, 2H), 3.02 (s, 6H), 2.95−2.87 (m, 4H), 2.63 (s, 4H), 2.51−2.28 (m, 3H), 2.10−2.05 (m, 3H), 1.80 (s, 4H), 1.71−1.44 (m, 4H), 0.97 (s, 3H). ^{13}C NMR (100 MHz, $CDCl_3$): δ 210.0, 156.8, 150.9, 137.7, 134.0, 132.3, 132.2, 130.9, 126.2, 123.4, 114.6, 112.2, 111.8, 66.9, 55.1, 54.6, 48.9, 47.6, 44.1, 40.1, 37.9, 31.8, 29.7, 29.2, 26.9, 26.0, 23.5, 14.7. HRMS (ESI): calcd for $C_{33}H_{43}N_2O_2$: $[M + H]^+$, 499.3319; found: $[M + H]^+$, 499.3323 (Δm = −0.0004 and error = −0.8 ppm).

(8*R*,9*S*,13*S*,14*S*)-16-((*E*)-4-Methoxybenzylidene)-13-methyl-3-(2-(pyrrolidin-1-yl)ethoxy)-6,7,8,9,11,12,13,14,15,16-decahydro-17*H*-cyclopenta-

https://doi.org/10.1021/acsomega.3c07574
ACS Omega 2024, 9, 6616−6626

[*a*]phenanthren-17-one (9). Compound **9** was prepared by employing method **B** by the reaction of compound **6** (100 mg, 0.25 mmol) and 2-chloroethyl pyrrolidine hydrochloride using a Cs_2CO_3 (325 mg, 1 mmol) base. The crude product was purified with the aid of column chromatography (8% MeOH in DCM) using silica gel to furnish pure compound **9** as a yellow solid; mp 235 to 237 °C; yield 84% (98 mg); R_f = 0.32 (80% ethyl acetate in pet ether). ^{1}H NMR (400 MHz, $CDCl_3$): δ 7.51 (d, J = 8.7 Hz, 2H), 7.42 (s, 1H), 7.2 (d, J = 8.5 Hz, 1H), 6.93 (d, J = 8.7 Hz, 2H), 6.70 (dd, J = 8.5, 2.6 Hz, 1H), 6.65 (d, J = 2.5 Hz, 1H), 4.41 (t, J = 4.7 Hz, 2H), 3.84 (s, 3H), 3.39 (t, J = 4.7 Hz, 2H), 3.3 (s, 3H), 2.97−2.83 (m, 3H), 2.53−2.45 (m, 1H), 2.42−2.38 (m, 1H), 2.28−2.26 (m, 1H), 2.10−2.08 (m, 6H), 1.70−1.67 (m, 1H), 1.59−1.52 (m, 3H), 1.48−1.43 (m,1H), 1.24 (s, 2H), 0.97 (s, 3H). ^{13}C NMR (100 MHz, $CDCl_3$): δ 209.7, 160.5, 155.5, 138.1, 133.5, 133.3, 133.1, 132.1, 128.3, 126.5, 114.4, 114.2, 112.4, 63.9, 55.4, 54.3, 54.1, 49.4, 47.7, 44.0, 37.8, 31.7, 29.6, 29.1, 26.7, 25.9, 23.3, 14.6. HRMS (ESI): calcd for $C_{32}H_{39}NO_3$: $[M + H]^+$, 486.3006; found: $[M + H]^+$, 486.3005 (Δm = +0.0001 and error = +0.6 ppm).

(8*R*,9*S*,13*S*,14*S*)-16-((*E*)-3,4-Dimethoxybenzylidene)-13-methyl-3-(2-(pyrrolidin-1-yl)ethoxy)-6,7,8,9,11,12,13,14,15,16-decahydro-17*H*-cyclopenta-[*a*]phenanthren-17-one (10). Compound **10** was synthesized by employing method **B** by reacting compound **7** (100 mg, 0.12 mmol) and 2-chloroethyl pyrrolidine hydrochloride in the presence of a Cs_2CO_3 (162 mg, 0.5 mmol) base. The crude product was purified using column chromatography (10% MeOH in DCM) over silica gel to afford pure compound **10** as a yellow solid; mp 240 to 245 °C; yield 80% (93 mg); R_f = 0.3 (76% ethyl acetate in pet ether). ^{1}H NMR (400 MHz, $CDCl_3$): δ 7.43 (s, 1H), 7.23−7.20 (m, 2H), 7.10 (d, J = 1.3 Hz, 1H), 6.94 (d, J = 8.3 Hz, 1H), 6.76 (dd, J = 8.6, 2.5 Hz, 1H), 6.70 (d, J = 2.3 Hz, 1H), 4.10 (t, J = 6.0 Hz, 2H), 3.94 (s, 5H), 2.97−2.88 (m, 6H), 2.62 (d, J = 6.3 Hz, 4H), 2.56−2.49 (m, 4H), 2.10−2.08 (m, 2H), 1.82−1.78 (m, 6H), 1.63−1.59 (m, 3H), 1.00 (s, 3H). ^{13}C NMR (100 MHz, $CDCl_3$): δ 209.7, 156.9, 150.1, 148.9, 137.6, 133.8, 133.3, 132.1, 128.6, 126.2, 123.9, 114.6, 113.2, 112.2, 111.1, 67.0, 55.9, 55.9, 55.1, 54.7, 48.6, 47.7, 44.1, 37.9, 31.7, 29.6, 29.0, 26.7, 25.9, 23.5, 14.6. HRMS (ESI): calcd for $C_{33}H_{41}NO_4$: $[M + H]^+$, 516.3126; found: $[M + H]^+$, 516.3125 (Δm = +0.0001 and error = +2.5 ppm).

1-(2-(((8*R*,9*S*,13*S*,14*S*)-16-((*E*)-4-(Dimethylammonio)-benzylidene)-13-methyl-17-oxo-7,8,9,11,12,13,14,15,16,17-decahydro-6*H*-cyclopenta-[*a*]phenanthren-3-yl)oxy)ethyl)pyrrolidin-1-ium. HCl (Est-1). **Est-1** ligand as a yellow solid was synthesized following method **C** by protonating compound **8** (30 mg, 0.06 mmol) with concentrated HCl (10 equiv) in the DCM solvent. mp 320 to 325 °C; yield 86% (29 mg); R_f = 0.3 (10% MeOH in DCM); ^{1}H NMR (400 MHz, CD_3CN): δ 11.63 (s, 1H), 7.69 (d, J = 8.3 Hz, 2H), 7.45 (s, 2H), 7.33 (s, 1H), 7.25 (d, J = 8.4 Hz, 1H), 6.76 (d, J = 8.6 Hz, 1H), 6.73(s, 1H), 4.37 (s, 2H), 3.64 (s, 2H), 3.34−3.39 (m, 3H), 3.06 (s, 6H), 2.98−2.89 (m, 3H), 2.60−2.42 (m, 2H), 2.09 (s, 6H), 1.62−1.51 (m, 2H), 1.34−1.27 (m, 4H), 1.12 (t, J = 7.0, 2H), 0.96 (s, 2H), 0.89 (t, J = 7.0, 3H). ^{13}C NMR (100 MHz, DMSO-d_6): δ 208.8, 155.9, 138.0, 133.2, 133.1, 132.5, 126.7, 114.9, 112.9, 112.7, 63.6, 53.9, 52.9, 48.5, 47.3, 43.9, 37.8, 31.9, 29.6, 29.2, 26.6, 26.0, 23.1, 14.9. HRMS (ESI): calcd for $C_{33}H_{44}N_2O_2$: $[M/2]^{2+}$, 250.1695; found: $[M/2]^{2+}$, 250.1679 (Δm = −0.0016 and error = −6.3 ppm).

1-(2-(((8*R*,9*S*,13*S*,14*S*)-16-((*E*)-4-Methoxybenzylidene)-13-methyl-17-oxo-7,8,9,11,12,13,14,15,16,17-decahydro-6*H*-cyclopenta[*a*]phenanthren-3-yl)oxy)-ethyl)pyrrolidin-1-ium. HCl (Est-2). **Est-2** ligand as a yellow solid was synthesized using method **C** by protonating compound **9** (50 mg, 0.1 mmol) with concentrated HCl in DCM solvent. mp 250 to 255 °C; yield 92% (49 mg); R_f = 0.44 (10% MeOH in DCM); ^{1}H NMR (400 MHz, $CDCl_3$): δ 12.65 (s, 1H), 7.52 (d, J = 8.6 Hz, 2H), 7.42 (s, 1H), 7.20 (d, J = 8.1 Hz, 1H), 6.94 (d, J = 8.6 Hz, 2H), 6.70 (d, J = 7.9 Hz, 1H), 6.66 (s, 1H), 4.48 (s, 2H), 3.84 (s, 5H), 3.48 (s, 2H), 2.98−2.92 (m, 5H), 2.53−2.37 (m, 2H), 2.29−2.23 (m, 3H), 2.08−2.06 (m, 4H), 1.74−1.64 (m, 1H), 1.58 (t, J = 8.6 Hz, 3H), 1.32−1.20 (m, 2H), 0.97 (s, 3H), 0.85 (t, J = 7.0 Hz, 1H). ^{13}C NMR (100 MHz, $CDCl_3$): δ 209.7, 160.5, 155.2, 138.1, 133.5, 133.1, 132.1, 128.3, 126.6, 114.3, 114.2, 112.4, 63.5, 55.4, 54.4, 54.1, 48.6, 47.7, 44.0, 37.8, 31.6, 29.6, 29.1, 26.7, 25.9, 23.3, 14.6. HRMS (ESI): calcd for $C_{32}H_{40}NO_3$: $[M]^+$, 486.3003; found: $[M]^+$, 486.3003 (Δm = 0.0000 and error = 0.0 ppm).

1-(2-(((8*R*,9*S*,13*S*,14*S*)-16-((*E*)-3,4-Dimethoxybenzylidene)-13-methyl-17-oxo-7,8,9,11,12,13,14,15,16,17-decahydro-6*H*-cyclopenta[*a*]phenanthren-3-yl)oxy)-ethyl)pyrrolidin-1-ium. HCl (Est-3). **Est-3** ligand as a yellow solid was prepared according to method **C** by protonating compound **10** (50 mg, 0.09 mmol) with concentrated HCl (10 equiv) in the DCM solvent. mp 265 to 270 °C; yield 90% (48 mg); R_f = 0.4 (10% MeOH in DCM); ^{1}H NMR (400 MHz, DMSO): δ 10.78 (s, 1H), 7.30 (s, 1H), 7.24 (t, J = 6.9 Hz, 3H), 7.05 (d, J = 8.2 Hz, 1H), 6.78 (dd, J = 8.5, 2.6 Hz, 1H), 6.73(d, J = 2.5 Hz, 1H), 4.30 (t, J = 4.9 Hz, 2H), 3.82 (d, J = 3.2 Hz, 8H), 3.57−3.53 (m, 5H), 3.11−3.07 (m, 3H), 2.92−2.87 (m, 3H), 2.03−1.87 (m, 6H), 1.55−1.48 (m, 4H), 0.91 (s, 3H). ^{13}C NMR (100 MHz, DMSO-d_6): δ 208.8, 155.9, 150.5, 149.1, 138.1, 134.3, 133.1, 132.8, 128.3, 126.7, 124.4, 114.9, 113.9, 112.8, 112.2, 63.6, 56.0, 55.9, 54.1, 53.6, 53.1, 48.4, 47.5, 43.9, 37.8, 31.8, 29.6, 28.9, 26.6, 26.0, 23.0, 14.8. HRMS (ESI): calcd for $C_{33}H_{42}NO_4$: $[M]^+$, 516.3108; found: $[M]^+$, 516.3106 (Δm = +0.0002 and error = +0.4 ppm).

Ligand Stock Solution Preparation. The 5 mM stock solution of **Est-1**, **Est-2**, and **Est-3** ligands was prepared in H_2O.

Oligonucleotides. The oligonucleotides (Tables S1 and S2, Supporting Information) utilized in all biophysical or biochemical studies were synthesized on a 1 μM scale as per the previously described procedure.[36] Deprotection of synthesized oligonucleotides was performed with aqueous methylamine (41%) and aqueous ammonia (30%, 1:1 v/v) heating at 65 °C for 30 min. Purification was carried out by 12% (*c-MYC*, mutated and telomeric DNA template) or 20% PAGE (*c-MYC*, *c-KIT1*, *h-RAS1*, telomeric, primer, and duplex DNA) containing 7 M urea and 10× TBE using standard protocols. Desalting of the purified DNAs was achieved with the help of the Sep-Pak column. Finally, the concentrations of all oligonucleotides were calculated with the PerkinElmer Lambda Bio+ UV−vis spectrophotometer at 260 nm wavelength employing appropriate molar extinction coefficients (ε).

CD Melting Studies. CD thermal melting profile was recorded in a quartz cuvette with a 1 mm path length on a JASCO-1500 CD spectrophotometer consisting of a PTC-423S temperature controller. The spectra were obtained at the 20−95 °C temperature range, with a heating rate of 1 °C min^{-1}. CD samples were prepared by dissolving 10 μM DNA in 10 mM lithium cacodylate buffer along with appropriate salt concentrations (1 mM KCl and 99 mM LiCl for *c-MYC* DNA; 50 mM KCl and 50 mM LiCl for *h-RAS1*; and 10 mM KCl and 90 mM LiCl for telomeric, *c-KIT*, and duplex DNA). The DNA

https://doi.org/10.1021/acsomega.3c07574
ACS Omega 2024, 9, 6616−6626

solutions were annealed by heating at 95 °C for 5 min and gradually cooling to room temperature over 3−4 h. After annealing, 5 mol equiv ligand concentrations were added to the DNA solution and kept overnight at 4 °C before recording the melting spectra at the fixed wavelength (263 nm for *c-KIT* and *c-MYC*; 295 nm for *h-RAS*; and 295 nm for telomeric and 242 nm for duplex DNA). The melting temperature ($T_{1/2}$) was then evaluated by analyzing the CD spectra by Origin 8.0 software using the Boltzmann function.[37]

CD Titration Studies. CD titration spectra were recorded in a quartz cuvette with a path length of 1 mm in the 200−600 wavelength range. The instrument parameters, such as scan speed 100 nm/min, response time 2 s, and bandwidth 2 nm, were kept constant for all the titration experiments. In the CD titration, 10 μM DNA samples were prepared in 10 mM lithium cacodylate buffer (7.2 pH) along with appropriate salt concentrations. The increasing molar concentrations of the ligand were added to the DNA samples and allowed to equilibrate for 3 min before recording the CD spectra. The baseline was corrected by using a buffer sample, and each CD spectrum was taken as an average of three accumulations. Finally, the CD spectra were examined through Origin 8.0 software.

***Taq* DNA Polymerase Stop Assay.** The *Taq* polymerase assay was executed using earlier reported procedures with trivial modifications.[36] FAM-labeled primer at 5′-end of *c-MYC*, mutated *c-MYC*, and telomeric DNA template are shown in Table S2, Supporting Information. A solution of 0.2 μM FAM-labeled primer and 0.1 μM DNA template was annealed by heating at 95 °C for 5 min in annealing buffer (5 mM Tris, pH 8.0, 10 mM NaCl, and 0.1 mM EDTA). The annealed primer-template DNA solution was then mixed with 1× polymerase buffer (50 mM Tris−HCl, pH 8.0, 0.5 mM DTT, 0.1 mM EDTA, 5 mM $MgCl_2$, 5 mM KCl, and 1 $\mu g\ \mu L^{-1}$ BSA in 5% glycerol). 0.2 mM dNTP solutions were added to this solution, and the entire reaction mixture was mixed gently. After this, an increasing concentration of **Est-3** (0−100 μM) was added to the reaction mixture (10 μL) and allowed to incubate at room temperature for 30 min. *Taq* DNA polymerase enzyme (1 U) was added to the final reaction mixtures and heated at 55 °C for 30 min to achieve the primer extension reaction. The progress of the reaction was then halted by adding 10 μL of loading dye (80% formamide, 1× TBE, 50 mM EDTA of 8.0 pH, and 0.025% bromophenol blue). The extension or stop products were separated on a 15% denaturing PAGE containing 7 M urea in 1× TBE (89 mM Tris−HCl and boric acid and 2 mM EDTA of pH 8.0 pH) running buffer. These products were visualized by scanning the gel on an Amersham Typhon 600 (GE Healthcare). Finally, the stop products were quantified with the aid of Image Quant 5.2 software. IC_{50} values were derived by plotting the percentage of the stop product against ligand concentrations using Origin 8.0 software.

Cell Culture. The HeLa and Lenti-X cell lines were cultured in Dulbecco's modified Eagle's minimum essential medium (DMEM), whereas the HepG2 cell line was grown in Eagle's minimum essential Medium (MEM) accompanied by 10% fetal bovine serum (FBS) and 1% antibiotic solution consisting of streptomycin and penicillin. All cell lines were maintained in an incubator (Memmert, ICO), having 5% CO_2 and 37 °C temperature.

Cell Viability Assay. The HeLa, HepG2, and Lenti-X cells were trypsinized and counted with the help of a hemocytometer. These cells were seeded in 96-well plates at a density of 10^4 per well, allowing them to reach confluency of up to 60−70% confluency. After 24 h, the medium was discarded and washed with 1× PBS (100 μL, pH 7.4) comprising 137 mM NaCl, 2.7 mM KCl, 10 mM Na_2HPO_4, and 1.8 mM KH_2PO_4. These cells were treated with increasing molar concentrations of **Est-3** (0−100 μM) and incubated for 24 h. Further, 100 μL of a 5 mg/mL MTT (HiMedia) medium solution was added to each well and incubated at 37 °C for over 4 h. 200 μL of DMSO was then added to each well and mixed using a rocker for 10 min to dissolve the insoluble formazan crystals. Once the formazan crystals dissolved, the absorbance was measured at 570 and 630 nm on a Thermo Scientific microplate reader (Multiskan Sky Microplate Spectrophotometer). IC_{50} values were then calculated by plotting the percentage cell viability against the logarithmic concentration ligand.[32] The resulting sigmoidal curve was finally fitted in the dose−response equation with the help of GraphPad Prism 8.3.0.[37]

RNA Extraction and Purification. In a six-well plate, approximately 1.5×10^5 HepG2 cells were seeded per well and allowed to adhere by keeping inside the incubator at 37 °C under the environment of 5% CO_2 for 24 h. After this, the cells were treated with an IC_{50} (∼5 μM) value of **Est-3** and further incubated for 48 h in the incubator under the same environment. After 48 h of **Est-3** treatment, the cells were washed with 500 μL of 1× PBS, trypsinized, and centrifuged to obtain the cell pellet. The cell pellet was used for RNA extraction and purification using the GeneJET RNA purification kit (Thermo Scientific, K0731) using the manufacturer's protocol. Last, the purified RNA was eluted from the column using 100 μL nuclease-free water and quantified by a nanophotometer (IMPLEN). The quantified RNA was further utilized as a template for cDNA synthesis.

cDNA Synthesis. cDNA synthesis was accomplished using a verso cDNA synthesis kit (Thermo Scientific, AB1453A) according to the manufacturer's protocol. A 20 μL reaction mixture in nuclease-free water was prepared by adding the 1× cDNA synthesis buffer (4 μL), 1 ng of RNA template, 500 ng of oligo dT primer (1 μL), RT enhancer (1 μL), 500 μM dNTP mix (2 μL), and verso enzyme mix (1 μL). The entire reaction mixture was initially heated at 42 °C for 30 min to make cDNA followed by heating at 92 °C for 2 min to inactivate the enzyme activity.

qRT-PCR Studies. The real-time quantitative PCR was carried out on an AriaMx Real-Time PCR instrument (Agilent Technologies) using a cDNA template and an ExcelTaq 2X Q-PCR Master Mix (SYBR, ROX) (SMOBIO, Catalog no. TQ110). Appropriate forward and reverse primers utilized in this study are shown in Table S3. The significant threshold value for both the housekeeping (β-actin) and the gene of interest (HepG2) was maintained within a suitable range (40 cycles). A 20 μL PCR sample was prepared by mixing the cDNA (1 μL), 0.4 μL of each forward and reverse primer (20 μM), and ExcelTaq 2X Q-PCR Master Mix (10 μL) in nuclease-free water (8.2 μL). The thermal cycle of PCR was set as follows: hot start at 95 °C for 3 min, 40 cycles of denaturation at 95 °C for 30 s, annealing at 57 °C for 30 s, and elongation at 72 °C for 30 s. Finally, the relative gene expression of the gene of interest (HepG2), together with the housekeeping gene (β-actin), was determined by the arithmetic calibrator $2^{(-\Delta\Delta Ct)}$ method.[37] Initially, the threshold values for both HepG2 and β-actin genes were acquired from the experiment. The error bars denote the standard deviations resulting from the three independent experiments. Statistical analysis was employed to estimate the

https://doi.org/10.1021/acsomega.3c07574
ACS Omega 2024, 9, 6616−6626

expression of the HepG2 gene in treated and untreated cells. The *p*-value was evaluated by the *t*-test with the help of GraphPad Prism 8.3.0. For the analysis, *p* values of less than 0.05 were considered significant.

Molecular Modeling and Dynamics Studies. The ligand was optimized at the HF/6-31G* theory level in Gaussian 16 software[38] and docked with *c-MYC* G4 DNA (PDB ID: 1XAV)[39] in AutoDock 4.2.6.[40] Lamarkian Genetic Algorithm was used to generate 500 docked conformers. ESP charges were calculated in Gaussian 16 for the docked conformers obtained from the most populated clusters, and RESP fitting[41] was carried out using the antechamber[42] module of AmberTools 19. MD studies were carried out using our previously reported protocol.[43] Briefly, the OL15,[44] GAFF,[45] and TIP3P force fields were used for the DNA, ligand, and water molecules, respectively, to generate the DNA: ligand complex in tleap. K^+ ions were used to neutralize the system in tleap. Further, 500 ns of the production run was conducted in the GPU-accelerated version of PMEMD[46−48] in AMBER 18.[49] All the analyses were performed using the CPPTRAJ[50] module of AmberTools 19, and the trajectory was visualized in VMD.[51] The "lie" command was used to calculate stacking energy and the vdW energy contribution and the "rdf" command for the radial distribution function. The binding energy was calculated using the molecular mechanics Poisson−Boltzmann surface area (MM/PBSA)[52] module of AMBER18 from the last 20 ns of the simulation. Images were rendered in PyMOL (Schrodinger LLC.).

■ ASSOCIATED CONTENT

Supporting Information

The Supporting Information is available free of charge at https://pubs.acs.org/doi/10.1021/acsomega.3c07574.

CD melting and titration curves, PAGE of *Taq* DNA polymerase stop assay, plots, and molecular modeling and dynamics studies, oligonucleotide sequences used in all studies, and copies of ^{1}H NMR and ^{13}C NMR spectra (PDF)

■ AUTHOR INFORMATION

Corresponding Author

Pushpangadan Indira Pradeepkumar − *Department of Chemistry, Indian Institute of Technology Bombay, Mumbai 400076, India;* orcid.org/0000-0001-9104-3708; Email: pradeep@chem.iitb.ac.in

Authors

Satendra Kumar − *Department of Chemistry, Indian Institute of Technology Bombay, Mumbai 400076, India*

Annyesha Biswas − *Department of Chemistry, Indian Institute of Technology Bombay, Mumbai 400076, India*

Sruthi Sudhakar − *Department of Chemistry, Indian Institute of Technology Bombay, Mumbai 400076, India*

Divya Kumari − *Department of Chemistry, Indian Institute of Technology Bombay, Mumbai 400076, India*

Complete contact information is available at: https://pubs.acs.org/10.1021/acsomega.3c07574

Notes

The authors declare no competing financial interest.

Dedicated to Professor Krishna N. Ganesh on the occasion of his 70th birthday.

■ ACKNOWLEDGMENTS

We are grateful to the Indian Institute of Technology Bombay for IITB-Spacetime-HPC resources and DST-FIST (grant no. SR/FST/CS-II/2017/37) for NMR and HRMS facilities. We appreciate Prof. Ruchi Anand and Prof. Shobhna Kapoor for giving us access to their laboratory facilities. S.K. thanks the UGC, IRCC-IIT Bombay, and Institute Postdoctoral Fellowship scheme for funding. A.B. thanks DST-Inspire and Institute Postdoctoral Fellowship, and S.S. thanks the Prime Minister Research Fellowship (PMRF) for Ph.D. fellowships.

■ REFERENCES

(1) Choi, J.; Majima, T. Conformational Changes of Non-B DNA. *Chem. Soc. Rev.* **2011**, *40* (12), 5893−5909.

(2) Chambers, V. S.; Marsico, G.; Boutell, J. M.; Di Antonio, M.; Smith, G. P.; Balasubramanian, S. High-Throughput Sequencing of DNA G-Quadruplex Structures in the Human Genome. *Nat. Biotechnol.* **2015**, *33* (8), 877−881.

(3) Neupane, A.; Chariker, J. H.; Rouchka, E. C. Structural and Functional Classification of G-Quadruplex Families within the Human Genome. *Genes (Basel)* **2023**, *14* (3), 645.

(4) Burge, S.; Parkinson, G. N.; Hazel, P.; Todd, A. K.; Neidle, S. Quadruplex DNA: Sequence, Topology and Structure. *Nucleic Acids Res.* **2006**, *34* (19), 5402−5415.

(5) Ma, Y.; Iida, K.; Nagasawa, K. Topologies of G-Quadruplex: Biological Functions and Regulation by Ligands. *Biochem. Biophys. Res. Commun.* **2020**, *531* (1), 3−17.

(6) Sanchez-Martin, V. DNA G-Quadruplex-Binding Proteins: An Updated Overview. *DNA* **2023**, *3* (1), 1−12.

(7) Huppert, J. L. Four-Stranded Nucleic Acids: Structure, Function and Targeting of G-Quadruplexes. *Chem. Soc. Rev.* **2008**, *37* (7), 1375−1384.

(8) Yuan, W. F.; Wan, L. Y.; Peng, H.; Zhong, Y. M.; Cai, W. L.; Zhang, Y. Q.; Ai, W. B.; Wu, J. F. The Influencing Factors and Functions of DNA G-Quadruplexes. *Cell Biochem. Funct.* **2020**, *38*, 524−532.

(9) Dai, J.; Carver, M.; Punchihewa, C.; Jones, R. A.; Yang, D. Structure of the Hybrid-2 Type Intramolecular Human Telomeric G-Quadruplex in K+ Solution: Insights into Structure Polymorphism of the Human Telomeric Sequence. *Nucleic Acids Res.* **2007**, *35* (15), 4927−4940.

(10) Tucker, B. A.; Hudson, J. S.; Ding, L.; Lewis, E.; Sheardy, R. D.; Kharlampieva, E.; Graves, D. Stability of the Na+ Form of the Human Telomeric G-Quadruplex: Role of Adenines in Stabilizing G-Quadruplex Structure. *ACS Omega* **2018**, *3* (1), 844−855.

(11) Wang, Y.; Patel, D. J. Solution Structure of the Human Telomeric Repeat d[AG3(T2AG3)3] G-Tetraplex. *Structure* **1993**, *1*, 263−282.

(12) Membrino, A.; Cogoi, S.; Pedersen, E. B.; Xodo, L. E. G4-DNA Formation in the HRAS Promoter and Rational Design of Decoy Oligonucleotides for Cancer Therapy. *PLoS One* **2011**, *6* (9), 24421.

(13) Dickerhoff, J.; Onel, B.; Chen, L.; Chen, Y.; Yang, D. Solution Structure of a MYC Promoter G-Quadruplex with 1:6:1 Loop Length. *ACS Omega* **2019**, *4* (2), 2533−2539.

(14) Hsu, S. T. D.; Varnai, P.; Bugaut, A.; Reszka, A. P.; Neidle, S.; Balasubramanian, S. A G-Rich Sequence within the c-Kit Oncogene Promoter Forms a Parallel G-Quadruplex Having Asymmetric G-Tetrad Dynamics. *J. Am. Chem. Soc.* **2009**, *131* (37), 13399−13409.

(15) Agrawal, P.; Lin, C.; Mathad, R. I.; Carver, M.; Yang, D. The Major G-Quadruplex Formed in the Human BCL-2 Proximal Promoter Adopts a Parallel Structure with a 13-Nt Loop in K+ Solution. *J. Am. Chem. Soc.* **2014**, *136* (5), 1750−1753.

(16) Chen, Y.; Agrawal, P.; Brown, R. V.; Hatzakis, E.; Hurley, L.; Yang, D. The Major G-Quadruplex Formed in the Human Platelet-Derived Growth Factor Receptor β Promoter Adopts a Novel Broken-Strand Structure in K+ Solution. *J. Am. Chem. Soc.* **2012**, *134* (32), 13220−13223.

(17) De Armond, R.; Wood, S.; Sun, D.; Hurley, L. H.; Ebbinghaus, S. W. Evidence for the Presence of a Guanine Quadruplex Forming

https://doi.org/10.1021/acsomega.3c07574
ACS Omega 2024, 9, 6616−6626

Region within a Polypurine Tract of the Hypoxia Inducible Factor 1α Promoter. *Biochemistry* **2005**, *44* (49), 16341−16350.
(18) Agrawal, P.; Hatzakis, E.; Guo, K.; Carver, M.; Yang, D. Solution Structure of the Major G-Quadruplex Formed in the Human VEGF Promoter in K+: Insights into Loop Interactions of the Parallel G-Quadruplexes. *Nucleic Acids Res.* **2013**, *41* (22), 10584−10592.
(19) Neidle, S. Quadruplex Nucleic Acids as Targets for Anticancer Therapeutics. *Nat. Rev. Chem* **2017**, *1*, 0041.
(20) Mendes, E.; Aljnadi, I. M.; Bahls, B.; Victor, B. L.; Paulo, A. Major Achievements in the Design of Quadruplex-Interactive Small Molecules. *Pharmaceuticals* **2022**, *15*, 300.
(21) Savva, L.; Georgiades, S. N. Recent Developments in Small-Molecule Ligands of Medicinal Relevance for Harnessing the Anticancer Potential of g-Quadruplexes. *Molecules* **2021**, *26* (4), 841.
(22) Xiong, Y. X.; Huang, Z. S.; Tan, J. H. Targeting G-Quadruplex Nucleic Acids with Heterocyclic Alkaloids and Their Derivatives. *Eur. J. Med. Chem.* **2015**, *97*, 538−551.
(23) Frasson, I.; Pirota, V.; Richter, S. N.; Doria, F. Multimeric G-Quadruplexes: A Review on Their Biological Roles and Targeting. *Int. J. Biol. Macromol.* **2022**, *204*, 89−102.
(24) Brassart, B.; Gomez, D.; Cian, A. D.; Paterski, R.; Montagnac, A.; Qui, K. H.; Temime-Smaali, N.; Trentesaux, C.; Mergny, J. L.; Gueritte, F.; Riou, J. F. A New Steroid Derivative Stabilizes G-Quadruplexes and Induces Telomere Uncapping in Human Tumor Cells. *Mol. Pharmacol.* **2007**, *72* (3), 631−640.
(25) Huang, S.; Liang, Y.; Cui, J.; Xie, J.; Liu, Y.; Hu, B.; Xiao, Q. Comparative Investigation of Binding Interactions with Three Steroidal Derivatives of d(GGGT)4 G-Quadruplex Aptamer. *Steroids* **2018**, *132*, 46−55.
(26) Bhutani, P.; Joshi, G.; Raja, N.; Bachhav, N.; Rajanna, P. K.; Bhutani, H.; Paul, A. T.; Kumar, R. U.S. FDA Approved Drugs from 2015-June 2020: A Perspective. *J. Med. Chem.* **2021**, *64* (5), 2339−2381.
(27) Shagufta; Ahmad, I.; Mathew, S.; Rahman, S. Recent Progress in Selective Estrogen Receptor Downregulators (SERDs) for the Treatment of Breast Cancer. *RSC Med. Chem.* **2020**, *11* (4), 438−454.
(28) Dhamodharan, V.; Pradeepkumar, P. I. Specific Recognition of Promoter G-Quadruplex DNAs by Small Molecule Ligands and Light-up Probes. *ACS Chem. Biol.* **2019**, *14* (10), 2102−2114.
(29) Allan, G. M.; Lawrence, H. R.; Cornet, J.; Bubert, C.; Fischer, D. S.; Vicker, N.; Smith, A.; Tutill, H. J.; Purohit, A.; Day, J. M.; Mahon, M. F.; Reed, M. J.; Potter, B. V. L. Modification of Estrone at the 6, 16, and 17 Positions: Novel Potent Inhibitors of 17β-Hydroxysteroid Dehydrogenase Type 1. *J. Med. Chem.* **2006**, *49* (4), 1325−1345.
(30) Carvalho, J.; Queiroz, J. A.; Cruz, C. Circular Dichroism of G-Quadruplex: A Laboratory Experiment for the Study of Topology and Ligand Binding. *J. Chem. Educ.* **2017**, *94* (10), 1547−1551.
(31) Głuszyńska, A.; Juskowiak, B.; Rubiś, B. Binding Study of the Fluorescent Carbazole Derivative with Human Telomeric G-Quadruplexes. *Molecules* **2018**, *23* (12), 3154.
(32) Ghasemi, M.; Turnbull, T.; Sebastian, S.; Kempson, I. The Mtt Assay: Utility, Limitations, Pitfalls, and Interpretation in Bulk and Single-Cell Analysis. *Int. J. Mol. Sci.* **2021**, *22* (23), 12827.
(33) Ocadiz, R.; Sauceda, R.; Cruz, M.; Graef, A. M.; Gariglio, P. High Correlation Between Molecular Alterations of the c-myc Oncogene and Carcinoma of the Uterine Cervix. *Cancer Res.* **1987**, *47* (15), 4173−4177.
(34) Fang, C.-H.; Gong, J.-Q.; Zhang, W. Function of Oval Cells in Hepatocellular Carcinoma in Rats. *World J. Gastroenterol.* **2004**, *10* (17), 2482−2487.
(35) Bookout, A. L.; Cummins, C. L.; Mangelsdorf, D. J.; Pesola, J. M.; Kramer, M. F. High-Throughput Real-Time Quantitative Reverse Transcription PCR. *Curr. Protoc. Mol. Biol.* **2006**, *73*, 15.8.1−15.8.28.
(36) Kumar, S.; Pany, S. P. P.; Sudhakar, S.; Singh, S. B.; Todankar, C. S.; Pradeepkumar, P. I. Targeting Parallel Topology of G-Quadruplex Structures by Indole-Fused Quindoline Scaffolds. *Biochemistry* **2022**, *61* (22), 2546−2559.
(37) Kumar, S.; Reddy Sannapureddi, R. K.; Todankar, C. S.; Ramanathan, R.; Biswas, A.; Sathyamoorthy, B.; Pradeepkumar, P. I. Bisindolylmaleimide Ligands Stabilize C-MYC G-Quadruplex DNA Structure and Downregulate Gene Expression. *Biochemistry* **2022**, *61* (11), 1064−1076.
(38) Frisch, M. J.; Trucks, G. W.; Schlegel, H. B.; Scuseria, G. E.; Robb, M. A.; Cheeseman, J. R.; Scalmani, G.; Barone, V.; Petersson, G. A.; Nakatsuji, H. *Gaussian 16*, Revision B. 01: Wallingford, CT, 2016.
(39) Ambrus, A.; Chen, D.; Dai, J.; Jones, R. A.; Yang, D. Solution Structure of the Biologically Relevant G-Quadruplex Element in the Human c-MYC Promoter. Implications for G-Quadruplex Stabilization. *Biochemistry* **2005**, *44* (6), 2048−2058.
(40) Morris, G. M.; Huey, R.; Lindstrom, W.; Sanner, M. F.; Belew, R. K.; Goodsell, D. S.; Olson, A. J. AutoDock4 and AutoDockTools4: Automated Docking with Selective Receptor Flexibility. *J. Comput. Chem.* **2009**, *30* (16), 2785−2791.
(41) Fox, T.; Kollman, P. A. Application of the RESP Methodology in the Parametrization of Organic Solvents. *J. Phys. Chem. B* **1998**, *102* (41), 8070−8079.
(42) Wang, J.; Wang, W.; Kollman, P. A.; Case, D. A. Automatic Atom Type and Bond Type Perception in Molecular Mechanical Calculations. *J. Mol. Graphics Modell.* **2006**, *25* (2), 247−260.
(43) Biswas, A.; Singh, S. B.; Todankar, C. S.; Sudhakar, S.; Pany, S. P. P.; Pradeepkumar, P. I. Stabilization and Fluorescence Light-up of G-Quadruplex Nucleic Acids Using Indolyl-Quinolinium Based Probes†. *Phys. Chem. Chem. Phys.* **2022**, *24* (10), 6238−6255.
(44) Galindo-Murillo, R.; Robertson, J. C.; Zgarbova, M.; Sponer, J.; Otyepka, M.; Jurečka, P.; Cheatham, T. E., III Assessing the Current State of Amber Force Field Modifications for DNA. *J. Chem. Theory Comput.* **2016**, *12* (8), 4114−4127.
(45) Wang, J.; Wolf, R. M.; Caldwell, J. W.; Kollman, P. A.; Case, D. A. Development and Testing of a General Amber Force Field. *J. Comput. Chem.* **2004**, *25* (9), 1157−1174.
(46) Götz, A. W.; Williamson, M. J.; Xu, D.; Poole, D.; Le Grand, S.; Walker, R. C. Routine Microsecond Molecular Dynamics Simulations with AMBER on GPUs. 1. Generalized Born. *J. Chem. Theory Comput.* **2012**, *8* (5), 1542−1555.
(47) Le Grand, S.; Götz, A. W.; Walker, R. C. SPFP: Speed without Compromise—A Mixed Precision Model for GPU Accelerated Molecular Dynamics Simulations. *Comput. Phys. Commun.* **2013**, *184* (2), 374−380.
(48) Salomon-Ferrer, R.; Gotz, A. W.; Poole, D.; Le Grand, S.; Walker, R. C. Routine Microsecond Molecular Dynamics Simulations with AMBER on GPUs. 2. Explicit Solvent Particle Mesh Ewald. *J. Chem. Theory Comput.* **2013**, *9* (9), 3878−3888.
(49) Case, D. A.; Aktulga, H. M.; Belfon, K.; Ben-Shalom, I.; Brozell, S. R.; Cerutti, D. S.; Cheatham, I. I. I.; T, E.; Cruzeiro, V. W. D.; Darden, T. A.; Duke, R. E. *Amber 2018*; University of California: San Francisco, 2018.
(50) Roe, D. R.; Cheatham, T. E., III PTRAJ and CPPTRAJ: Software for Processing and Analysis of Molecular Dynamics Trajectory Data. *J. Chem. Theory Comput.* **2013**, *9* (7), 3084−3095.
(51) Humphrey, W.; Dalke, A.; Schulten, K. VMD: Visual Molecular Dynamics. *J. Mol. Graphics* **1996**, *14* (1), 33−38.
(52) Kollman, P. A.; Massova, I.; Reyes, C.; Kuhn, B.; Huo, S.; Chong, L.; Lee, M.; Lee, T.; Duan, Y.; Wang, W.; et al. Calculating Structures and Free Energies of Complex Molecules: Combining Molecular Mechanics and Continuum Models. *Acc. Chem. Res.* **2000**, *33* (12), 889−897.

https://doi.org/10.1021/acsomega.3c07574
ACS Omega 2024, 9, 6616−6626